Delineation of Sedimentary Basin Structure beneath the Banyumas Basin, Central Java, Indonesia, Using Ambient Seismic Noise Tomography

Ahmad Setiawan (ahmad.setiawan@esdm.go.id)
Ministry of Energy and Mineral Resources: Kementerian Energi dan Sumber Daya Mineral
https://orcid.org/0000-0001-6201-5249
Zulfakriza Zulfakriza
ITB: Institut Teknologi Bandung
Andri Dian Nugraha
ITB: Institut Teknologi Bandung
Shindy Rosalia
ITB: Institut Teknologi Bandung
Awali Priyono
ITB: Institut Teknologi Bandung
Sri Widiyantoro
ITB: Institut Teknologi Bandung
David P. Sahara
ITB: Institut Teknologi Bandung
Marjiyono Marjiyono
Kementerian Energi dan Sumber Daya Mineral
Januar H. Setiawan
ESDM: Kementerian Energi dan Sumber Daya Mineral
Eko Budi Lelono
Kementerian Energi dan Sumber Daya Mineral
Asep K. Permana
Kementerian Energi dan Sumber Daya Mineral
Hidayat Hidayat
Kementerian Energi dan Sumber Daya Mineral

Research Article

Keywords: Banyumas sedimentary basin, volcanic area, hydrocarbon, Ambient Noise Tomography, cross-correlation, Green's Function, Rayleigh wave, shear wave.

Posted Date: March 18th, 2021

DOI: https://doi.org/10.21203/rs.3.rs-314198/v1

Abstract

Subsurface images of an area with a thick volcanic layer generally can not be well-imaged with conventional seismic exploration (seismic reflection) due to seismic wave scattering. Another method is needed to obtain an accurate subsurface image in a thick volcanic layer area. In this study, we applied Ambient Noise Tomography (ANT) to image the shear-wave velocity (Vs) structure in the Banyumas Basin, Central Java, Indonesia, which has relatively thick volcanic layers. We aimed to delineate the sediment deposits and the sedimentary thickness in this area. Although this method has limited application for subsurface imaging with a thick volcanic layer area, the application of cross-correlations from ambient noise has been widely applied in numerous locations to obtain greater understanding of subsurface structures. In this study, more than 1,000 pairs of vertical component cross-correlations were used to estimate the Green's Function of the Rayleigh wave. The Multiple Filter Technique (MFT) was used as a Time-Frequency Analysis and 1,291 dispersion curves were obtained. The Neighbourhood Algorithm (NA) was utilized to inverse the dispersion curves at 121 grid points which were used to obtain a vertical depth profile of 1D Vs. The Vs map results show that the low Vs tend to trend in a northwest-southeast direction associated with two areas: the Majenang low, and the Citanduy low. The presence of low Vs values corresponds with Middle Miocene–Pliocene sedimentary rocks. Meanwhile, the high Vs value in this area might correspond with Oligocene–Early Miocene volcanic products and Eocene sediment. Our study was also able to reveal the thickness of sedimentary rocks in the the Banyumas sedimentary basin, which is believed to have hydrocarbon potential.

1. Introduction

Java Island is located in the Indonesian archipelago and has unique geological features due to its subducting plate zone. The existence of a recent volcanic arc on the island is a result of interactions between the Eurasian and Indo-Australian Plates in the southern part of Java. The Indo-Australian Plate moves relatively north, perpendicular to Java Island since the Late Cretaceous era (Hall 2012), subducting beneath the Eurasian Plate with a convergence rate of 67 mm yr^{-1} (Simon et al. 2007). This tectonic activity has caused the development of faults and basins in the area, which are important for oil and gas plays.

Situmorang et al. (1976) suggest that the northward lateral compression force from the Indian oceanic plate and the southward lateral compression force from the Sundaland block present a wrench fault tectonism on Java Island, as first explained by Moody and Hill (1956). Due to these forces, pairs of strike-slip faults developed in opposite directions which meet in southern Central Java and caused the geological settings in Central Java to become more complex than those of West and East Java (Satyana 2007). These faults have also modified the petroleum geology in Central Java, which generally developed in the forearc and backarc basins, as is present on Sumatra Island and on other parts of Java Island (Satyana 2007).

Our study area is Banyumas Basin, which is one of the inter-mountainous sedimentary basins located in the south of Central Java (Fig. 1). Oil and gas seepage can be found in several locations in the Banyumas Basin, which indicate an active petroleum system (Satyana 2007). The status of this area is still in the exploration stage; as the result, many researchers are attracted to commence research in this area, especially regarding the petroleum geology. Previous studies regarding the petroleum system in Banyumas Basin have been widely discussed; e.g., see Noeradi et al. 2006; Subroto et al. (2007 and 2008); and Setiawan et al. 2018.

Studies using geophysical methods that cover the Banyumas Basin area have also been carried out in Central Java, Indonesia. Based on the map of horizontal gravity gradient anomaly, the formation of sedimentary basins in the south of Central Java has a northwest-southeast and northeast-southwest direction (Widianto 2008). A study of seismic reflection has also been conducted in this area. However, the seismic image results give a poor image of the subsurface structures in the Banyumas Basin due to the relatively thick volcanic deposits. In 2018, the Center for Geological Survey (PSG), Geological Agency, Indonesia, conducted an integrated survey using surface geology to identify elements of the petroleum system and geophysics to image the subsurface geological structure of the Banyumas Basin. Based on physical parameters of the rock density using gravity studies, Hidayat et al. (2020) also show the delineation of the Citanduy sub-basin and the Majenang sub-basin.

The relatively thick volcanic deposits present our main challenge in obtaining good subsurface images of this basin. Therefore, we attempted to apply another imaging method in this study, especially at shallow depths. We used Ambient Noise Tomography (ANT) to obtain a precise subsurface image of the Banyumas Basin. ANT has been widely used by geophysicists to image shallow subsurface structures and has resulted in better vertical resolutions, complementing the results of body wave tomography using global data (Widiyantoro and van der Hilst 1996) and regional data (Rosalia et al. 2019).

ANT uses the cross-correlation of ambient seismic noise data records between two pair stations to obtain the Empirical Green's Function (EGF), which is associated with surface waves (Snieder and Wapenaar 2010; Paul et al. 2005; Snieder 2004; Wapenaar et al. 2010). ANT has been used extensively to image crustal structures in countries worldwide: Australia (Saygin and Kennet 2010), the Netherlands (Yudistira et al. 2017), China (Liu et al. 2016; Liu et al. 2017), Scotland (Nicolson et al. 2012), Tibet (Jiang et al. 2014; Zheng et al. 2017; Yao et al. 2009), and the United States (Ritzwoller et al. 2011). ANT has also been applied in Indonesia to determine S-wave velocity structures in West Java (Rosalia et al. 2020), Central Java (Zulfakriza et al. 2014), East Java (Martha et al. 2017), the Bandung Basin (Wuryani et al. 2019; Pranata et al. 2020), as well as on the islands of Bali (Zulfakriza et al. 2020), and Lombok (Sarjan et al. 2020), and the Banda Arc (Porritt et al. 2016).

ANT studies of a sedimentary basin area are relatively limited in Indonesia, especially in a basin that has a thick volcanic layer. Although the ANT regional study done by Rosalia et al. (2020) includes the Banyumas Basin, as well as the northwest-southeast trending regional structure, these results could not describe the subsurface images of the Banyumas Basin in detail. In this study, we use a greater number

of local ambient seismic noise data sets recorded by 68 local stations with 60 days of observation between June and July 2018 to obtain more detail images in Banyumas basin. We aimed to delineate the sediment deposits which characterized by the low Vs pattern and present a vertical shear wave velocity structure beneath the Banyumas Basin, as well as to determine the thickness of the sedimentary rocks in the area. Our results are usefull in providing additional knowledge regarding the exploration challenges in the Banyumas Basin.

2. Geological Settings

Geologically, the study area (Fig. 1) is predominantly covered with alluvial deposits and sedimentary rocks from the Halang Formation. The sedimentary rocks of the Halang Formation consist of tuffaceous sandstones, conglomerates, marlies, clay stones, and andesitic breccias at the bottom level (Kastowo and Suwarna 1996). There are also volcaniclastic products from the Kumbang Formation of the same age as that of the Halang Formation (Middle Miocene-Pliocene), which consist of volcanic breccias, lava, dykes, and tuffs composed of andesite and basalt. The Kumbang Formation connects with the Halang Formation and overlaps the Kalipucang Limestone (Middle Miocene). Above the sequential Halang Formation are several Pliocene formations, which consist of : the Kalibiuk Formation, which consists of clay and marlite deposits; the Kaliglagah Formation, which consists of coarse sandstone and conglomerate deposits; and the Tapak Formation, which consist of coarse sandstone sediment with marl intercalations. Quarterly volcanic products and alluvium deposits can be found at the top of these formations.

The older formation underneath the Halang Formation consists of the Rambatan Formation, the Pemali Formation (the term “Penanjung Formation” was first used by Setiawan (2019), the Nusakambangan Formation, and the Jampang/Gabon Formation. The Rambatan Formation (Middle Miocene) consists of sedimentary sandstone and conglomerate with marl and shale. The Pemali Formation (Middle Miocene) consists of sedimentary deposits of tuffaceous sandstones and sandy limestone. The Nusakambangan Formation (Early Miocene) consists of tuff sediments with sandstone insertions. The Gabon Formation (Oligocene-Early Miocene) consists of breccia volcaniclastic deposits with pieces of andesite in a tuff/sand matrix. The geological map of the survey area (Fig. 1) reveals that the Halang, Kumbang, and Tapak Formations, as well as the alluvial deposits, tend to trend in a northwest-southeast direction.

3. Data And Method

3.1 Data

In this study, waveform data from the seismic network deployed by the Center for Geological Survey (PSG), Geological Agency, Indonesia, was used. The seismic network used 68 portable 3-C broadband borehole seismic stations in an area of less than 0.5 square degrees within the Banyumas Basin area, which is south of Central Java, Indonesia (Fig. 1). The data used was from the records of June and July 2018. The minimum and maximum distances between the seismometer stations are 5 and 6 km,

respectively. The waveform data was collected every two weeks; the batteries were replaced, and the seismometers checked in the same two-week timeframe. In this study, we utilized only those Rayleigh waves that were obtained from the cross-correlation results of the noise data between station pairs. As a result, only the vertical component of the waveform data was used in the processing steps.

Several steps were first carried out before each seismometer was installed. First, a drillhole at the location of the seismometer station was drilled; these averaged a depth of 16 meters. Secondly, the base of the borehole was cemented with mortar to make it easier to securely couple the seismometer. Thirdly, a 2.5 inch diameter pipe was inserted into the drill hole. Fourthly, the seismometer was inserted into the drill hole. The last step was filling the pipe with water to reduce noise from human activities.

To ensure safekeeping, the seismometers were located in the yards of selected residents, while the recording instruments were placed inside their houses. The seismic data was recorded and stored on a 16 GB removable flash disk (micro SD card). A real-time GPS was also connected to each recording instrument to record data in real-time. Another process that was also carried out was differential GPS measurements above the location of each of the seismometers to determine the location and height of the seismometer locations in greater detail.

3.2 Ambient noise cross-correlation and group velocity extraction

Ambient seismic noise interferometry refers to the process of cross-correlation between two sets of ambient seismic noise data that is recorded by two receivers in an acoustic diffusion wavefield to produce EGF at the receiver position as if one of the stations acts as the source (Wapeenar et al. 2006; Wapeenaar et al. 2010; Curtis 2006). Ambient seismic noise data recording has an advantage since it does not require earthquake sources, which means it can be measured at any time and anywhere (Curtis 2006; Yang and Ritzwoller 2008). Yang and Ritzwoller (2008) also show that ambient noise sources generally take place over a short period (<20s) and are considered to be related to the interaction between ocean waves near the coastline and the ocean floor. Generally, two maximum-sized peaks of short-term seismic noise were observed in the primary (10-20s) and secondary microseismic (5-10s) time ranges.

The procedure for preprocessing ambient seismic noise data follows Bensen et al. (2007), while the steps used to produce the EGF of the Rayleigh wave follow those of Saygin and Kennet (2010), which were also used by Zulfakriza (2014 and 2020). The cross-correlation process between two stations, X_A and X_B, as stated by Saygin and Kennet (2010), could be written as:

$$G(X_A, X_B, t) = \int_{-\infty}^{\infty} v_1(X_A, \tau) v_2(X_B, t+\tau) d\tau \qquad (1)$$

Where $v_1(X_A, t)$ dan $v_2(X_B, t)$ represents the seismic data recorded at stations A and B, t is the time variable, and τ is the lag time.

In this study, we produced 2,278 potential cross-correlation pairs from 68 broadband portable stations, using 60 days of continuous data, in order to determine the Vs velocity structure beneath the Banyumas sedimentary basin. Because this study only used a vertical component of seismic data, Rayleigh waves were the type of surface waves obtained from the cross-correlation process. We applied a narrow Gaussian band to each EGF to determine the arrival time of the Rayleigh waves (Fig. 2A).

Surface waves have a unique dispersive characteristic that occurs when the velocity is a function of period or frequency. We can measure the value of the surface wave velocity of different frequencies using a dispersion curve. The EGF Rayleigh surface waves were obtained from the cross-correlation of data records between station pairs containing information about the velocity of the surface wave propagation in terms of frequency or time period. The Multiple Filtering Technique (MFT), introduced by Dziewonskie et al. (1969), was used to analyze the EGF and produce a Rayleigh surface wave dispersion curve for the medium between the station pairs. MFT is conducted by manually picking the maximum peak of the amplitude of the Rayleigh surface wave envelope. The dispersion curve obtained is then used for the tomographic inversion of the velocity of the Rayleigh wave group for each period.

From 2,278 potential EGF, we chose only those EGF that were clear enough to use in the dispersion curve analysis. EGF that were too noisy were not used for further processing. We rejected more than 1,000 EGF and used only 1,291 EGF to produce a Rayleigh wave dispersion curve (Supplementary Fig. S1), which was done by manually picking the amplitude peak of the Rayleigh wave envelope in the fundamental mode (Fig. 2B-C).

3.3 Group velocity inversion

In this study, we used the Fast Marching Surface Tomography (FMST) package from Rawlinson (2005) to obtain variations in the Rayleigh surface wave velocity. The Fast Marching Method (FMM) was used for the forward problem and the subspace scheme was used at the inversion stage. FMM is a grid-based schema for solving eikonal equations, using a finite-difference based on Rawlinson and Sambridge (2005), which is the most effective method of accurately tracking waveforms to determine the travel time of ray paths passing through a medium at heterogeneous velocities. The subspace inversion method is also an iterative method, part of a class of highly-effective algorithms that minimizes objective/misfit functions using a quadratic approximation of the parameter space model in a relatively small dimension (Kennett et al.1988). This method has been successfully applied to produce velocity variation maps of the Rayleigh group (Saygin and Kennet 2010; Martha et al. 2017; Zulfakriza et al. 2020).

The objective functions S(m) that are minimized during the inversion process can be written as follows:

$$S(m) = (g(m) - d_{obs})^T C_d^{-1} (g(m) - d_{obs}) + \varepsilon (m - m_0)^T C_m^{-1} (m - m_0) + \eta m^T D^T D m \qquad (2)$$

Where m is an unknown model parameter vector (such as group velocity), g(m) is the predicted travel time of the group velocity, d is the observed travel time of the group velocity, C_d is the covariance data

matrix, m_0 is the reference model, C_m is the model parameter covariance matrix, D is a smoothness matrix, e is a damping parameter, and h is a smoothing parameter.

3.4 Depth inversion

We applied the Neighbourhood Algorithm (NA) introduced by Sambridge (1999a, b) to determine the variation of 1D shear wave velocity from the surface wave dispersion curve inversion. NA is a nonlinear inversion method classified as a direct search method and is considered capable of solving inversion problems that have quite complex relationships between observational data and unknown model parameters. The NA direct search inversion method is divided into two stages. First, the search stage, which samples multi-dimensional parameter space to find a combination of model parameters that are suitable for observational data. Second, the appraisal stage which extracts information from the complete ensemble of collected models to find a single optimal model. The search algorithm used by NA is in the same classification as the GA and SA techniques; namely, randomly searching for the decision function of the misfit instead of using derivative calculations in the misfit data function (free-derivative misfit function).

Wathelet et al. (2008) successfully applied NA to produce new computer code for creating inversions of Rayleigh surface wave dispersion curves. The NA inversion algorithm was also used by Zulfakriza et al. (2020) to produce variations in velocity Vs to describe tomography beneath the Agung-Batur volcanic complex on Bali Island.

In this study, we used the Vp of checkshot velocity data obtained from measurements at the Jati-1 well location (Fig. 1) as the initial search model. The depth of the well from the recorded check shot information is approximately 4.3 km with a Vp value range from 2.5 km/s to 3.3 km/s. We obtained the Vs value of the Jati-1 well by applying the empirical ratio of Vp/Vs 1.74 which was calculated from travel time tomography data processing (Hidayat 2020). We also used a velocity model from CRUST 1.0 (Laske et al. 2013) which is limited to the second layer and crystal crust 1 at a depth of 11.66 km. The minimum and maximum Vs values obtained from the CRUST 1.0 model are 0.88 km/s and 3.4 km/s, respectively.

4. Results

4.1. Checkerboard resolution test

We used a Checkerboard Resolution Test (CRT) in a checkerboard pattern of low and high velocity groups as an initial model to determine how well the study area could be recovered. We conducted several checkerboard cell sizes to test the proper resolution sizes as indicated by the checkerboard pattern's recovery in this study. The optimum cell sizes were then applied to each period to obtain the tomographic image of the velocity of the Rayleigh wave group.

We conducted three checkerboard resolution tests using different cell dimensions: ~8.5km x 8.5km, ~ 6.5km x 6.5km, and ~ 5.5km x 5.5km, as shown in Fig. 3. The three CRT experiments all used the same

parameter. The results showed good recovery of the checkerboard pattern on the inside of the station network, compared to outside the station network. The checkerboard recovery results using a ~ 5.5km^2 cell size show a smearing effect compared to the other cell sizes. Therefore, we decided to use the ~ 6.5km^2 grid cell size as the optimum resolution size to be recovered in the study area. By using a ~ 6.5km^2 grid cell size, we expected to image the study area's complex geological conditions in greater detail, as compared to previous studies.

Damping and smoothing parameters are important parameters for solving the optimum solution of the inversion of Eq. 1. We tested the damping parameter values of 10 – 5,000 and the smoothing parameter values of 5 – 3,000 through the trade-off curve (Supplementary Fig. S2) and obtained an optimum value of 300 and 300, respectively. The supplementary S3 image shows the results of the checkerboard resolution test at different periods, using a ~ 6.5km^2 grid cell size, a damping parameter of 300, and a smoothing parameter of 300. The results show that the checkerboard recovery pattern is sufficient in periods 1s to 6s. In contrast, in periods higher than 6s, the recovery pattern is insufficient for indicating a recovery of the checkerboard pattern.

4.2. Rayleigh wave group velocity maps

Tomographic inversion was performed on the observed travel time data extracted from the dispersion curve to determine the variation in velocity of the Rayleigh wave group in periods 1 to 6s. Figure 4 shows the distribution map of the velocity variation of the Rayleigh wave group in the study area in periods 1 to 6s. The parameter used is the same as that was used in the optimum CRT. The map of the Rayleigh wave group velocity result in a high resolution velocity model inside the station network due to the large numbers and the high density of the raypaths (shown in the inset map of Fig. 4). In this study, a longer period than 6s was not used because 6s already has a low resolution which relates to the reduced amount of ray path coverage (Supplementary Fig. S4).

The geological features of the group velocity map of the Rayleigh wave in Fig. 4 show the presence of two low group velocity values which are separated by high group velocity and have northwest-southeast trending structures. The low group velocity might correspond to relatively thick sedimentary rocks in the area which is evidenced by the distribution of alluvial sedimentary layer, the Halang, Kumbang, and Tapak Formations and coincide with the depocenter of the Majenang Low (northwest) and the Citanduy Low (southeast). In addition to the high group velocity anomaly that separates the two low group velocity, other high group velocities are also present in the southwest and northeast.

4.3. Shear wave velocity model

We successfully applied the NA algorithm, introduced by Sambridge (1999a, b), to produce a 2-D profile of shear wave velocity maps at each depth (Fig. 6). The Rayleigh wave dispersion curve obtained from the group velocity map for each period (1-6s) was then extracted to obtain a dispersion curve at 121 points, which was evenly distributed at intervals of 0.05^o (~ 5.5km) in the study area.

The inversion of the 1D shear wave velocity (Vs) model was carried out on 121 grid point dispersion curves that had previously been made using a dinver package, part of the Geopsy software developed by Wathelet et al. (2008). The inversion results produced 1D Vs profiles (Fig. 5). The results of the 1D Vs profile produced velocity information (Vs) at different depths, dependent on the consistency of the dispersion curve at the selected grid points.

Several parameters need to be determined in the 1-D Vs inversion process; e.g., the total thickness model for the Earth's layer, the range of velocity of the search model, and the range of thickness of the Earth's layer. In this study, we used five layers of parameters for the NA inversion process with different velocity values of Vs and depth thickness. The range of uniform Vs model parameters used for each layer were: 500-1,300 m/s, 700-2,000 m/s, 1,000–2,300 m/s, 1,400-2,500 m/s, and 2,000–3,500 m/s. The model parameters for the thickness of each layer were: 200-1,290 m (bottom depth), with the other three layers in the thickness range of: 1,290-1,500 m, 1,500-2,000 m, and 2,000–4,000 m.

Figure 5A-C shows three examples of the 1D Vs vertical profile obtained by applying the Neighborhood Algorithm. Figure 5D shows the location of three examples of 1D Vs. Figure 5A shows a gradual increase in the Vs values with increasing depth from the surface, as can be seen in the 1D Vs profile in Fig. 5B-C. After the inversion of the dispersion curve on all 121 grid points, we did an interpolation to obtain a 2D Vs map at depths of 0.5-8 km (Fig. 6). The low *Vs* pattern that appears on the velocity map of the Rayleigh wave group velocity is consistent with the map of Vs value distribution to a depth of 3 km (Fig. 6A-D) and tends to trend in the northwest-southeast direction; whereas higher Vs are dominant at depths of more than 3 km.

5. Discussion

The results of the 1-D profile inversion of Vs (Fig. 5) show a rock layer with an increasing velocity structure; i.e., each Vs value is higher than in the previous layer. We show the 1-D profile inversion from 3 different location in Fig. 5: in the northern part which characterized with high group velocity (Fig. 5A), and in the Majenang Low (Fig. 5B) and the Citanduy Low (Fig. 5C) which both characterized with low group velocity. The Vs value is reached at depth of 8,000 m in Fig. 5A, which is about 2,700 m/s, shallower than the Vs value that was achieved in Fig. 5B-C. This shows the possibility that rock layers with higher velocity structures can be found at shallower depths than in Fig. 5B-C. From Fig. 5, we also observed that there is a possibility that the response tendency of the low anomaly Vs extends to the middle of the study area.

Figure 5B-C is likely to be in a response area having the value of Vs in an area covered by Quaternary deposits that trend northwest-southeast. Based on the response of the value of Vs produced at the same depth of 8,000 m, Fig. 5B produces a Vs response value up to 2,500 m/s, while Fig. 6C produces a response value of Vs up to 2,200 m/s. This indicates the possibility of thicker sedimentary layers leading southeast. In Fig. 5A-C, it also can be seen that the highest Vs value obtained starts at a depth of ~ 6,000 m, along with the possibility of a rock structure discontinuity limit of the highest velocity value that can

be found in the study area. We also note that the dispersion calculation curve in the fundamental mode of Fig. 5A-C is not very fit, following the change in velocity at 0.6-1 Hz frequencies. This indicates that the computational limitations in the frequency range are dependent on the grid size used. Since we used a grid size of ~ 6.5 km^2, this indicates that a geological object sized less than ~ 6.5 km^2 cannot be properly resolved.

The explanation of the results from Fig. 5 can be clarified by the 2D Vs profile in Fig. 6. The low anomaly Vs (0.4–1.7 km/s) is estimated as the response of the Middle Miocene-Pliocene rock distribution (Kumbang, Halang, and Tapak Formations). At the same time, the response of the quaternary rocks, which is likely at a depth range of 0–0.5 km, cannot be resolved from ANT results. The medium anomaly Vs (1.71 km/s – 2.3 km/s) is estimated as a response of Early-Middle Miocene sedimentary rocks (Nusakambangan, Penanjung, and Rambatan Formations). At the same time, the high anomaly (2.31 km/s – 2.7 km/s) was estimated as a response of the Oligocene-Early Miocene rocks (volcanic products of the Gabon Formation).

In the tomogram map of the Vs model in Fig. 6, it can be seen that the pattern of low-velocity trends northwest-southeast. This is interpreted as a low Vs area of the Majenang Low and the Citanduy Low, respectively. The Majenang Low is located relatively north of the study area, and the Citanduy Low is located south of the study area. The depocenter of the Majenang and Citanduy Lows are also seen in the Vs tomogram map at depths of 0.5 km to 3 km.

5.1. Vertical cross-section

We present a vertical cross-section that is west-east (Fig. 7) and south-north (Fig. 8) in order to detect the Vs structure of the study area at depths of 0.5-8 km. In this study, we utilize the facies analysis of the Jati-1 well logs data from Junursyah (2018) (Supplementary Table S1) for the interpretation of the Vs results from ANT. Supplementary Table S1 illustrates the bottom and top position limits of each formation that can be interpreted from the Jati-1 well logs. The vertical profile crossing the A-A' lines in Fig. 7A cross the Jati-1 well. The bottom limit of the Halang Formation, or the top of the Rambatan Formation, possibly corresponds to the lower limit of the contrast value of the first layer Vs (~ 0.8–1.7 km/s) of the A-A' vertical profile in Fig. 7A.

The bottom of the Penanjung Formation, or the top of the Nusakambangan Formation, is in contrast to the value of the second layer Vs (~ 1.7–2.3 km/s) of the vertical profile of the A-A' in Fig. 7A. The third layer of the A-A vertical section has a value of Vs > 2.3 km/s and is estimated to be a response of rocks older than the Nusakambangan Formation. Explanations of the first, second, and third layers in Fig. 7A (lines B-B') and Fig. 8 (lines C-C' and D-D') follow the vertical cross-section of lines A-A.'

The vertical interpretation of the rock response to the Vs value is described in Figs. 7 and 8. The first layer is interpreted as Middle Miocene-Pliocene rock response (Kumbang, Halang, and Tapak Formations), and the second layer is interpreted as the Early-Middle Miocene rock response (Nusakambangan, Penanjung, and Rambatan Formations). Based on the results of oil-to-source rock correlation, Subroto et al. (2007)

and Setiawan et al. (2018) estimate the existence of Eocene sediment which has potential as source rock in the Banyumas Basin, indicating the possible existence of further rock layers beneath the Gabon Formation. The third layer of the A-A' vertical section is estimated to be the response of volcanic products from the Gabon Formation (Oligocene–Early Miocene) and Eocene sediment. A very high contrast value of Vs could not be obtained from our tomographic results, so it is possible that our tomographic results do not cover the basement of the Banyumas Basin, which is older than the Eocene period.

Setiawan et al. (2018) state that the volcanic data obtained, namely the Gabon Formation, shows tholeiitic affinity and has a basaltic composition that is associated with an oceanic island/volcanic arc. At the same time, Christensen and Stanley (2003) show that the value of Vp and Vs for each type of rock; the results of their study also show the minimum Vp and Vs values for basaltic rocks, which is about 5.9 km/s and 3.2 km/s. From these studies, we estimate that the results of ANT studies in the study area have not yet reached the basement because the highest Vs value that can be achieved is still lower than the Vs value obtained by Christensen and Stanley (2003).

5.2. Comparison of ANT results with other methods

We also compared ANT results with geophysical and geological methods, in addition to correlations using data facies analysis from the Jati-1 well logs (Fig. 7A), as seen in Fig. 9. From the results of the Vs tomogram model (Fig. 9A), two patterns of low Vs anomaly in the study area were obtained; these are located in a relatively northwest-southeast direction and separated by the Cipari Anticline; namely, the Majenang Low and Citanduy Low. The depocenter of the Majenang Low is estimated to be northwest of the area, while the depocenter of the Citanduy Low is estimated to be southeast of the area. These are marked by Vs anomaly values that are lower than the surrounding points. The pattern and direction of the low Vs are relatively the same as the pattern of the low bouguer anomaly shown in Fig. 9B. The strike slip faults southwest and northeast of the study area are interpreted as the Citanduy and the Karangbolong Faults. This interpretation is reinforced by Muchsin et al. (2002), as shown in Fig. 9C.

6. Conclusions

The ambient noise cross-correlation technique was successfully applied to the vertical component data of the seismic records carried out in the Banyumas sedimentary basin to produce the EFG of a Rayleigh wave. The characteristic of the ambient noise source obtained in this area is in the secondary microseismic range (5s-10s period). ANT was able to delineate the subsurface structure of the Banyumas Basin, shown on the variations of Vs value at depths of 0.5 km to 8 km. Based on the map of variations in the value of Vs, there are two low Vs value, which are interpreted as the Majenang Low and the Citanduy Low, respectively.

By utilizing the facies analysis of the Jati-1 well logs data from Junursyah (2018), we found three layers of subsurface structures in the Banyumas Basin that could be seen from the ANT results. The first layer, with a value of Vs 0.8 km/s – 1.7 km/s, is estimated to be a response from rocks of the Middle Miocene-Pliocene and consists of the Kumbang, Halang, and Tapak Formations. The second layer, with a value of

Vs 1.71 km/s – 2.3 km/s, is estimated to be related to rocks of the Early-Middle Miocene and consists of the sediment of the Nusakambangan, Penanjung, and Rambatan Formations. The third layer, with a value of Vs 2.31 km/s – 2.7 km/s, is estimated to consist of sedimentary rock of the Eocene and the Early Oligocene-Miocene of Gabon Formation. Our findings could be used as additional information for hydrocarbon exploration in the Banyumas Basin.

Declarations

Acknowledgements

We would like to thank Center for Geological Survey (PSG), Geological Agency, Indonesia for the waveform data used in this study. Some of figures presented were plotted using Generic Mapping Tools (Wessel and Smith 1998).

Availability of data and materials

Vs data will be shared through the PSG, Geological Agency, Indonesia website after this paper is published

Funding

This study was supported by the Ministry of Energy and Mineral Resources, Indonesia, for its scholarship, the ITB Research Program 2019-2020, the Master's Thesis Research Program BP-PTNBH Kemristek/BRIN 2020, and World Class Research Kemristek/BRIN Program 2021-2022 awarded to ADN. The study was also partially supported by and the Center for Earthquake Science and Technology, Research Center for Disaster Mitigation, Institut Teknologi Bandung (CEST, PPMB, ITB).

Authors' contributions

A.S., Z.Z., A.D.N., S.R., A.P., S.W., D.P.S. contributing to the data processing, interpretation, and writing of the manuscript. A.S., M.M., J.H.S., E.B.L., A.K.P., and H.H. conceived the seismic survey in Banyumas basin area. All authors contributed to the preparation of the manuscript. All authors have read and approved the final manuscript.

Competing Interests Statement

We declare that we have no significant competing financial, professional or personal interests that might have influenced the performance or presentation of the work described in this manuscript.

References

Asikin S, Handoyo A, Prastistho B, Gafoer S (1992) Peta Geologi Lembar Banyumas, Jawa, Skala 1:100.000. Pusat Penelitian dan Pengembangan Geologi, Bandung

Badan Geologi (2009) Peta Cekungan Sedimen Indonesia. Badan Geologi, Bandung

Bensen GD, Ritzwoller MH, Barmin MP, Levshin AL, Lin F, Moschetti MP, Shapiro NM, Yang Y (2007) Processing seismic ambient noise data to obtain reliable broad-band surface wave dispersion measurements. Geophys J Int 169:1239–1260. doi:10.1111/j.1365-246X.2007.03374.x

Christensen NI, Stanley D (2003) Seismic Velocities and Densities of Rocks. International Handbook of Earthquake and Engineering Seismology 81B**:** 1587-1594

Curtis A, Gerstoft P, Sato H, Snieder R, Wapenaar K (2006) Seismic interferometry-turning noise into signal. The leading edge, pp 1082-1092

Djuri M, Samodra H, Amin TC, Gafoer S (1996) Peta Geologi Lembar Purwokerto dan Tegal, Skala 1:100.000. Pusat Penelitian dan Pengembangan Geologi, Bandung

Dziewonski AS, Bloch S, Landisman M (1969) A technique for the analysis of transient seismic signals. Bull Seismol Soc Am 59:427–444. doi:10.1016/j.ultras.2008.12.001

Hall R (2012) Late Jurassic–Cenozoic reconstructions of the Indonesian region and the Indian Ocean. Tectonophysics 570-571:1-41. doi:10.1016/j.tecto.2012.04.021

Hidayat H (2020) Delineasi Struktur Kecepatan Seismik 3-D pada Cekungan Banyumas, Jawa Tengah, Menggunakan Tomografi Waktu Tempuh. Tesis Program Magister, Institut Teknologi Bandung

Hidayat H, Subagio S, Praromadani ZSA (2020) Interpretasi Struktur Geologi Bawah Permukaan Berdasarkan Updating Data Gaya Berat Cekungan Banyumas, Jawa Tengah. Jurnal Geologi dan Sumberdaya Mineral 21(3):111-118. doi:10.33332/jgsm.geologi.21.3.111-118p

Herrmann RB (2013) Computer programs in seismology. an evolving tool for instruction and research. Seismol Res Lett 84:1081-1088. doi:10.1785/0220110096

Jiang M, Ai Y, Zhou S, Chen YJ (2014) Distribution of the low velocity bulk in the middle-to-lower crust of the southern Tibet. implications for formation of the north-south trending rift zones. Earthq Sci 27(2)**:**149-157. doi:10.1007/s11589-014-0080-1

Junursyah GML (2018) The Integration of Gravity, Magnetotelluric, Magnetic and Seismic Data in Delineating the Banyumas Basin, unpublished reports. Pusat Survei Geologi, Bandung

Kastowo, Suwarna N (1996) Peta Geologi Lembar Majenang, Jawa, Skala 1:100.000 Edisi ke-2. Pusat Penelitian dan Pengembangan Geologi, Bandung

Kennett BLN, Sambridge MS, Williamson PR (1988) Subspace methods for large scale inverse problems involving multiple parameter classes. Geophysical Journal 94: 237–247. doi: 10.1111/j.1365-246x.1988.tb05898.x

Laske G, masters G, Ma Z, Pasyanos M (2013) Update on CRUST1.0 – A 1-degree global model of Earth's crust. Geophysical Research Abstract 15**:** 2658

Liu C, Yao H (2017) Surface Wave Tomography with Spatially Varying Smoothing Based on Continuous Model Regionalization. Pure Appl Geophys 174**:**937-953. doi: 10.1007/s00024-016-1434-5

Liu Z, Huang J, Yao H (2016) Anisotropic Rapyleigh wave tomography of Northeast China using ambient seismic noise. Physics of the Earth and Planetary Interiors 256:37-48. http.//dx.doi.org/10.1016/j.pepi.2016. 05.001

Martha AA, Cummins P, Saygin E, Widiyantoro S, Masturyono (2017) Imaging of upper crustal structure beneath East Java-Bali, Indonesia with ambient noise tomography. Geoscience letters 4(14):1-12. doi:10.1186/ s40562-017-0080-9

Moody JD, Hill MJ (1956) Wrench fault tectonics. Geological Society of America. Bulletin 67:1207-1246

Muchsin N, Ryacudu R, Kunto TW, Budiyani S, Yulianto B, Wiyanto B, Nurjayadi A, Raharjo K, Riandra F (2002) Miocene hydrocarbon system of the Southern Central Java region. In: Proceeding of 31st Annual Convention of Indonesian Association of Geologists

Nicolson H, Curtis A, Baptie B, Galetti E (2012) Seismic interferometry and ambient noise tomography in the British Isles. Proceedings of the Geologists' Association 123:74-86. doi:10.1016/j.pgeola.2011.04.002

Noeradi D, Subroto EA, Wahono HE, Hermanto E, Zaim Y (2006) Basin evolution and hydrocarbon potential of Majalengka-Bumiayu transpression basin, Java Island, Indonesia. In: AAPG International Conference and Exhibition, Perth, West Australia

Paul A, Campilo M, Margerin L, Larose E, Derode A (2005) Empirical synthesis of time-asymmetrical Green functions from the correlation of coda waves. Journal of Geophysics Research 110:1-13. doi:10.1029/2004JB003521

Porritt RW, Miller MS, O'Driscoll LJ, Harris CW, Roosmawati N, da Costa LT (2016) Continent-arc Collision in the Banda Arc imaged by ambient noise tomography. Earth and Planetary Science Letters 449:246-258. https://dx.doi.org/10.1016/j.epsl.2016.06.011

Pranata B, Yudistira T, Widiyantoro S, Brahmantyo B, Cummins PR, Saygin E, Zulfakriza Z, Rosalia S, Cipta A (2020) Shear wave velocity structure beneath Bandung basin, West Java, Indonesia from Ambient Noise Tomography. Geophysical Journal International 220(2):1045-1054. https://doi.org/10.1093/gji/ggz493

Rawlinson N, Sambridge M (2005) The fast marching method. an effective tool for tomographic imaging and tracking multiple phases in complex layered media. Exploration Geophysics 36: 341 – 350

Rawlinson N (2005) FMST. Fast Marching Surface Tomography Package, Canberra . Research School of Earth Science, Australian National University

Ritzwoller MH, Lin FC, Shen W (2011) Ambient noise tomography with a large seismic array. Comptes Rendus Geoscience 343:558-570. doi:10.1016/j.crte.2011.03.007

Rosalia S, Widiyantoro S, Nugraha AD, Suspendi P (2019) Double-difference tomography of P- and S-wave velocity structure beneath the western part of Java, Indonesia. Earthquake Science 32:12-25. doi: 10.29382/eqs-2019-0012-2

Rosalia S (2020) Crustal Structure Imaging Beneath Western Java Using Seismic Ambient Noise Tomography. Disertasi Program Doktor, Institut Teknologi Bandung

Sambridge M (1999a) Geophysical inversion with a neighborhood algorithm I. Searching a parameter space. Geophys J Int 138:479–494. doi:10.1046/j.1365- 246x.1999.00876.x

Sambridge M (1999b) Geophysical inversion with a neighborhood algorithm II. Appraising the ensemble. Geophys J Int 138:727–746. doi:10.1046/j.1365- 246x.1999.00900.x

Sarjan AFN, Zulfakriza Z, Nugraha AD, Rosalia S, Wei S, Widiyantoro S, Cummins PR, Muzli M, Sahara DP, Puspito NT, Priyono A, Afif H (2020) Delineation of Upper Crustal Structure Beneath the Island of Lombok, Indonesia, Using Ambient Seismic Noise Tomography. Frontiers in Earth Science (Under Revision)

Satyana AH (2007) Central Java, Indonesia – A "Terra Incognita" in petroleum exploration: new consideration on the tectonic evolution and petroleum implications. In: Proceedings of Indonesian Petroleum Association, Thirty-First Annual Convention and Exhibition

Saygin E, Kennett BLN (2010) Ambient seismic noise tomography of Australian continent. Tectonophysics 481:116 – 125. doi:10.1016/j.tecto. 2008.11.013

Setiawan R, Patriani EY, Yurnaldi D, Asmoro P, Sukapti S (2018) Stratigrafi Cekungan Banyumas, unpublished reports. Pusat Survei Geologi, Badan Geologi, Bandung

Setiawan R (2019) Sistem hidrokarbon pada tatanan vulkanik. Konsep dan studi kasus. Publikasi khusus eksplorasi hidrokarbon di sistem vulkanik. Pusat Survei Geologi, Badan Geologi, Bandung

Simandjuntak TO, Surono (1992) Peta Geologi Lembar Pangandaran, Jawa, Skala 1:100.000. Pusat Penelitian dan Pengembangan Geologi, Bandung, Indonesia

Simons WJF, Socquet A, Vigny C, Ambrosius BAC, Abu SH, Promthong C, Subarya C, Sarsito DA, Mathussen S, Morgan P, Spakman W (2007) A decade of GPS in Southeast Asia: Resolving Sundaland motion and boundaries. J Geophys Res 112:B06420. doi:10.1029/2005JB003868

Situmorang B, Siswoyo, Thajib E, Paltrinieri F (1976) Wrench Fault Tectonics and Aspects of Hydrocarbon Accumulation in Java. In: Proceedings of Indonesia Petroelum Association (IPA), Fifth Annual Convention, pp 53-66

Snieder R (2004) Extracting the Green's function from the correlation of coda waves. A derivation based on stasionary phase. Physical Review 69:1-18. doi:10.1103/PhysRevE.69.046610

Snieder R, Wapenaar K (2010) Imaging with ambient noise. Physic Today 63**:**44-49. doi:10.1063/1.3490500

Stein S, Wysession M (2003) An introduction to seismology, earthquake, and earth structure. Blackwell Publishing*,* Oxford, pp 86-101

Subroto EA, Noeradi D, Priyono A, Wahono HE, Hermanto E, Praptisih, Santoso K (2007) The paleogene basin with the Kendeng Zone, Central Java island, and implications to hydocarbon prospectivity. In: Proceedings of Indonesian Petroleum Association, Thirty-first Annual Convention & Exhibition

Subroto EA, Ibrahim A, Hermanto E, Noeradi D (2008) Contribution of Paleogene and Neogene sediments to the petroleum system in the Banyumas sub-basin, southern Central Java, Indonesia. In: AAPG International Conference and Exhibition, Cape Town, South Africa, pp 1-6

Wapenaar K, Draganov D, Robertsson J (2006) Introduction to supplement on seismic interferometry. Geophysics 71(4):1-4

Wapenaar K, Draganov D, Snieder R, Campman X, Verdel A (2010) Tutorial on seismic interferometry. Part 1 – Basic principles and applications. Geophysics 75(5):195-209. doi: 10.1190/1.3457445

Wathelet M, Jongmans D, Ohrnberger M, Bonnefoy-Claudet S (2008) Array performances for ambient vibrations on a shallow structure and consequences over Vs inversion. J Seismol 12:1–19. doi: 10.1007/s10950-007- 9067- x

Widianto E (2008) Penentuan Konfigurasi Struktur Batuan Dasar dan Jenis Cekungan dengan Data Gayaberat serta Implikasinya pada Target Eksplorasi Minyak dan Gas Bumi di Pulau Jawa*.* Disertasi Program Doktor, Institut Teknologi Bandung

Widiyantoro S, van der Hilst R (1996) Structure and evolution of the lithospheric slab beneath the Sunda Arc, Indonesia. Science 271:1566-1570

Wuryani SD, Yudistira T, Widiyantoro S (2019) Surface wave tomography using seismic ambient noise data for subsurface imaging beneath Bandung basin, West Java and its surrounding. In: IOP Conference Series. Earth and Environtmental Science

Yang Y, Ritzwoller MH (2008) Characteristics of ambient seismic noise as a source for surface wave tomography. Geochemistry Geophysics Geosystems *9*(2):1-18. doi:10.1029/2007GC001814

Yao H, Campman X, Hoop MV, Hilts RD (2009) Estimation of surface wave Green's functions from correlation of direct waves, coda waves, and ambient noise in SE Tibet. Physics of the Earth and Planetary Interiors 177:1-11. doi:10.1016/j.pepi.2009.07.002

Yudistira T, Paulssen H, Trampert J (2017) The crustal structure beneath The Netherlands derived from ambeint seismic noise. Tectonophysics 721:361-371. http./dx.doi.org/10.1016/j.tecto.2017.09.025

Zheng DC, Saygin E, Cummins P, Ge Z, Min Z, Cipta A, Yang R (2017) Transdimensional Bayesian seismic ambient noise tomography across SE Tibet. Journal of Asian Earth Sciences 134:86-93. http.//dx.doi.org.10.1016.j.jseaes.2016.11.011

Zulfakriza Z, Saygin E, Cummins PR, Widiyantoro, S, Nugraha AD, Lühr BG, Bodin T (2014) Upper crustal structure of central Java, Indonesia, from transdimensional seismic ambient noise tomography. Geophysical Journal International 197:630–635. doi:10.1093/gji/ ggu016

Zulfakriza Z, Nugraha AD, Widiyantoro S, Cummins PR, Sahara DP, Rosalia S, Priyono A, Kasbani K, Syahbana DK, Priambodo IC, Martanto M, Ardianto A, Husni YM, Lesmana A, Kusumawati D, Prabowo BS (2020) Tomography Imaging of the Agung-Batur Volcano Complex, Bali, Indonesia, From the Ambient Seismic Noise Field. Frontiers in Earth Science 8(43):1-11. doi:10.3389/feart.2020. 00043

Figures

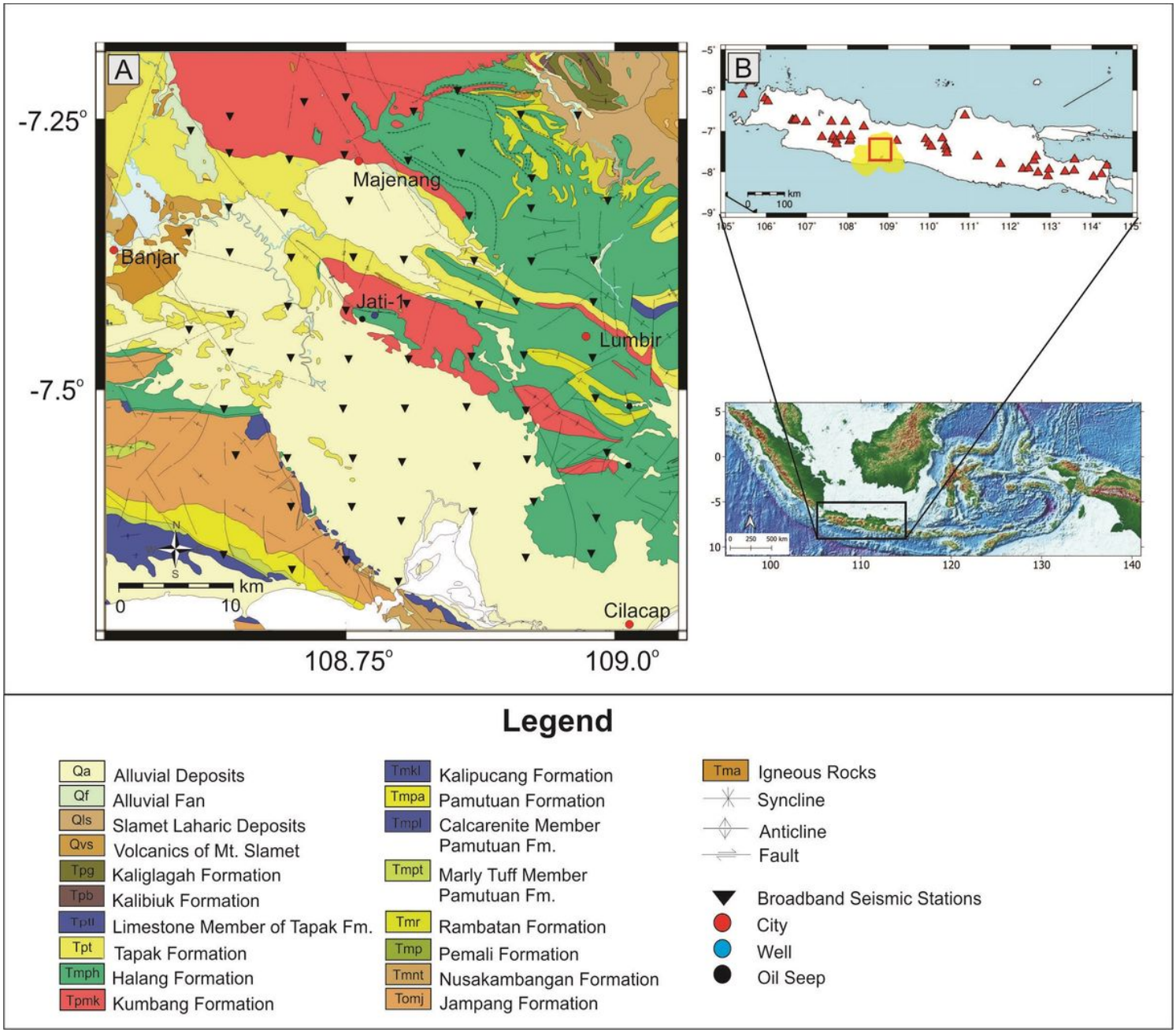

Figure 1

A Geological map of the study area (modified from Simandjuntak and Surono 1992; Kastowo and Suwarna 1996; Djuri et al. 1996; Asikin et al. 1992) ; B Insert map of survey location. The yellow area is the Banyumas Basin (Badan Geologi, 2009), the red square shows the survey location, and the red triangle is a volcano on Java Island

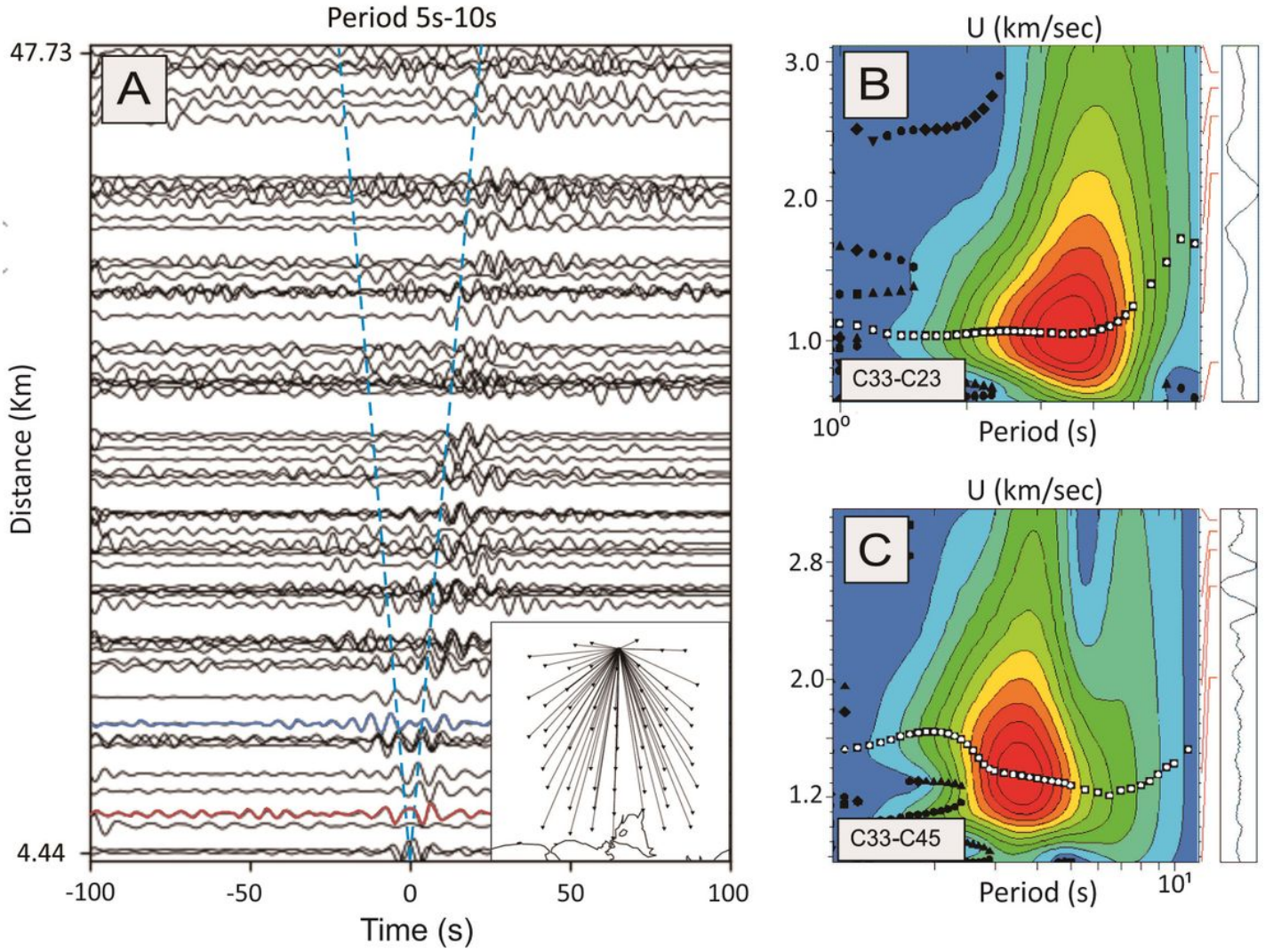

Figure 2

A Cross-correlogram between station pairs C33 against all possible receiving stations with an average Rayleigh wave velocity of 2.12 km/s. The position between station C33 and the other stations is indicated on the inset map. The dashed blue line indicates the lagtime trend of the Rayleigh EGF waves as the distance between stations increased. The blue wave signal indicates the result of cross-correlation between stations C33-C23, while the red wave signal indicates the result of cross-correlation between stations C33-C45; B-C The dispersion curve of the EGF picking process between stations C33-C23 and C33-C45. The white dot indicates the result of group velocity picked at the top of the envelope, with the red sphere denoting the maximum energy possessed by the Rayleigh wave

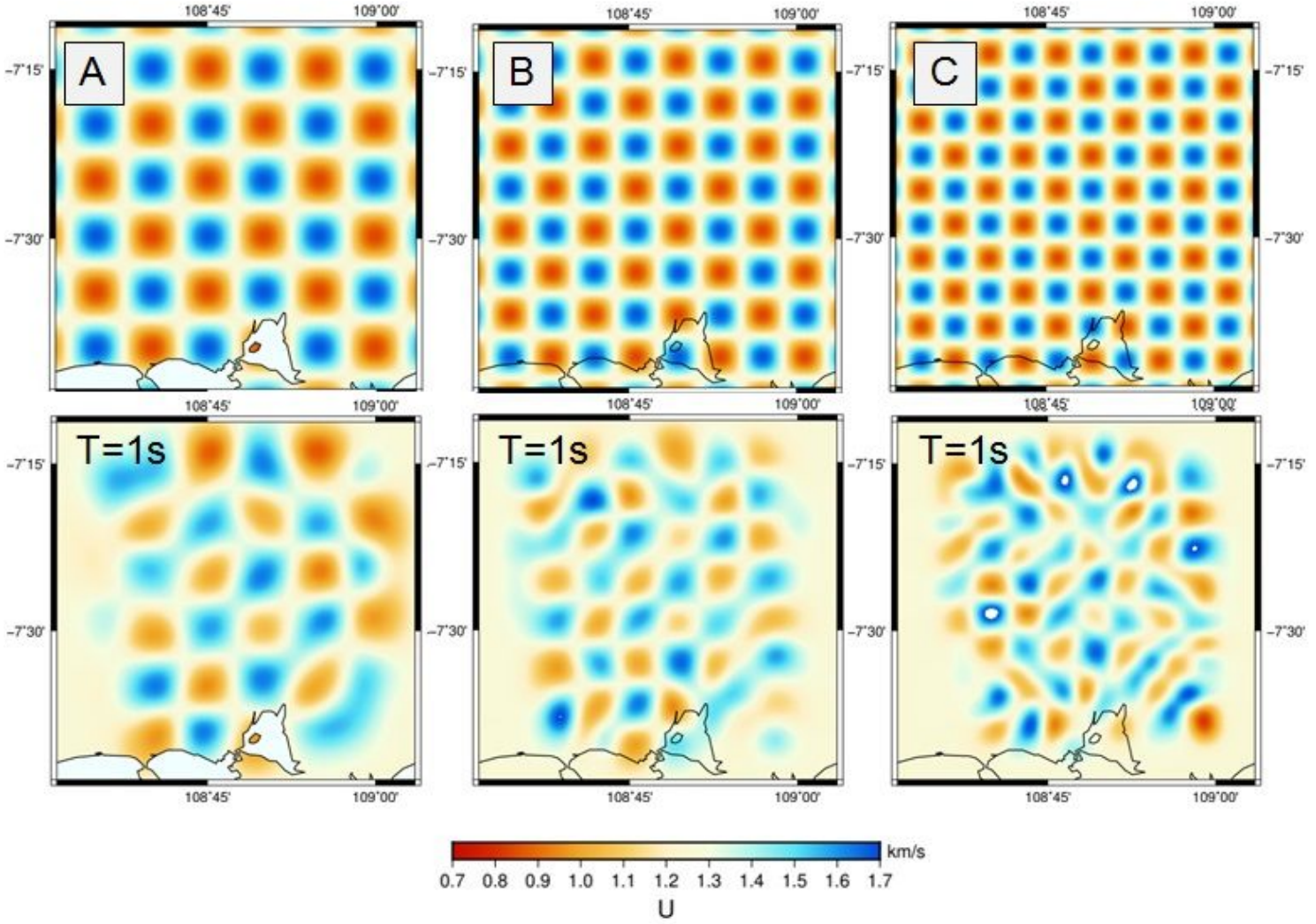

Figure 3

A-C Synthetic Rayleigh wave group velocity models for each cell grid size, ranging between ~8.5 km x 8.5 km, ~6.5km x 6.5km, and ~5.5 km x 5.5 km; and the final model obtained after applying the checkerboard resolution test for period 1s of the synthetic model, showing the distribution of stations in the study area.

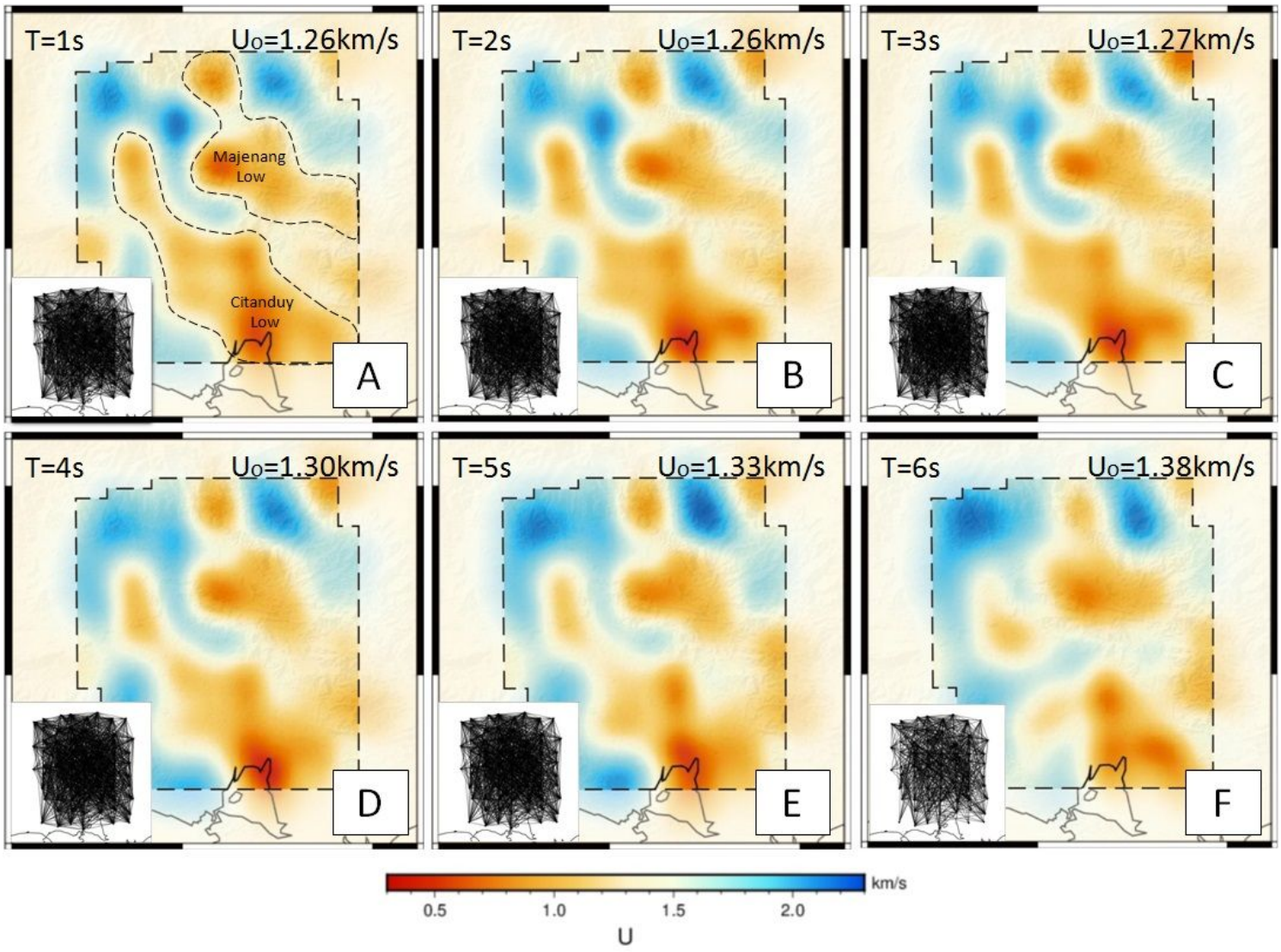

Figure 4

A-F The Rayleigh wave group velocity map at periods 1 to 6s and the raypath shown in the insert map. The low group velocity, high group velocity and the developing structures in this area tend to trend northwest-southeast

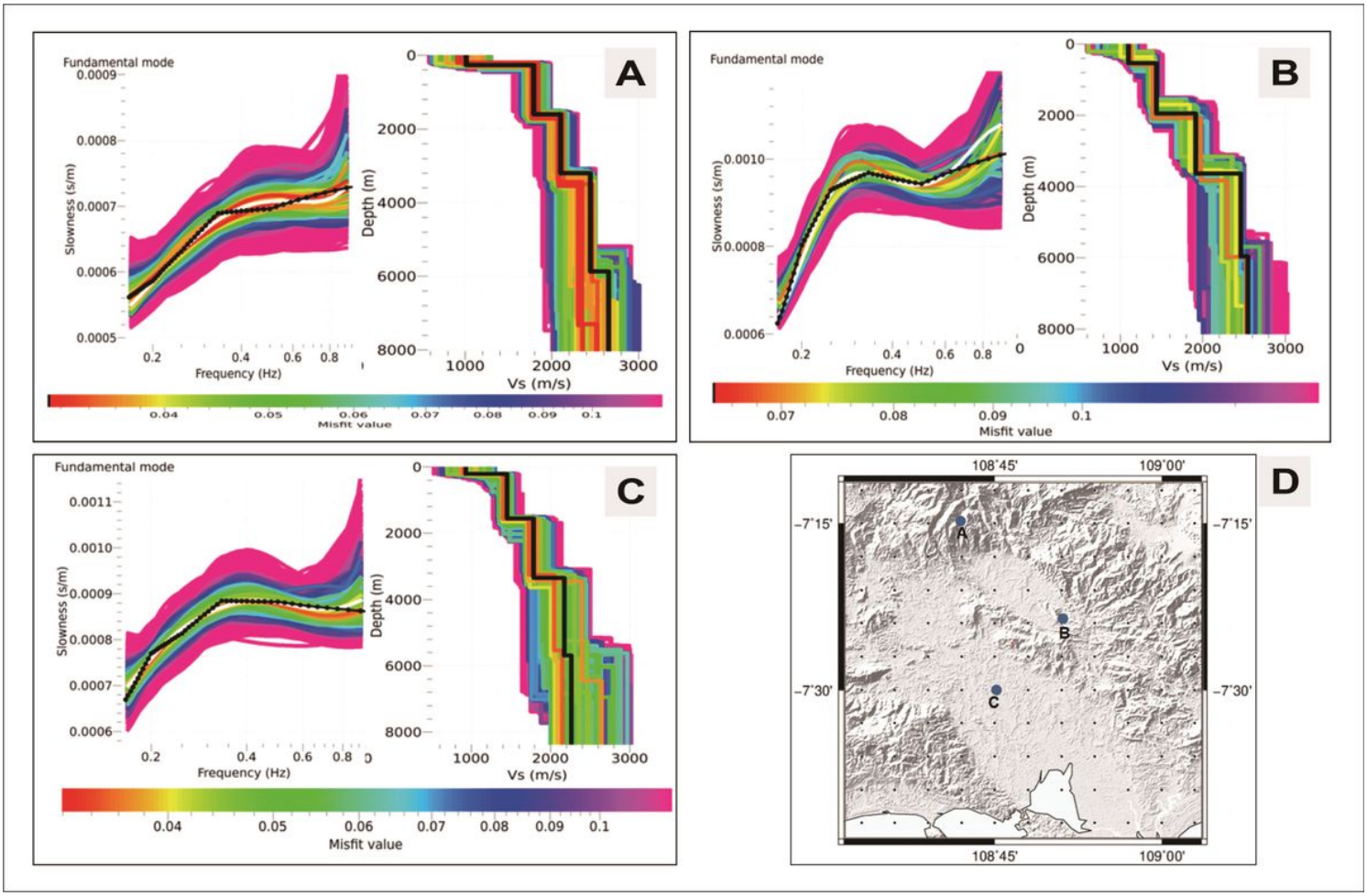

Figure 5

A-C Three examples of dispersion curve inversions at three different locations; D Coordinates of three examples (denoted by blue dots) of the application of dispersion curve inversion in the study area. Small, gray dots denote the 121 grid points of the dispersion curve inversion

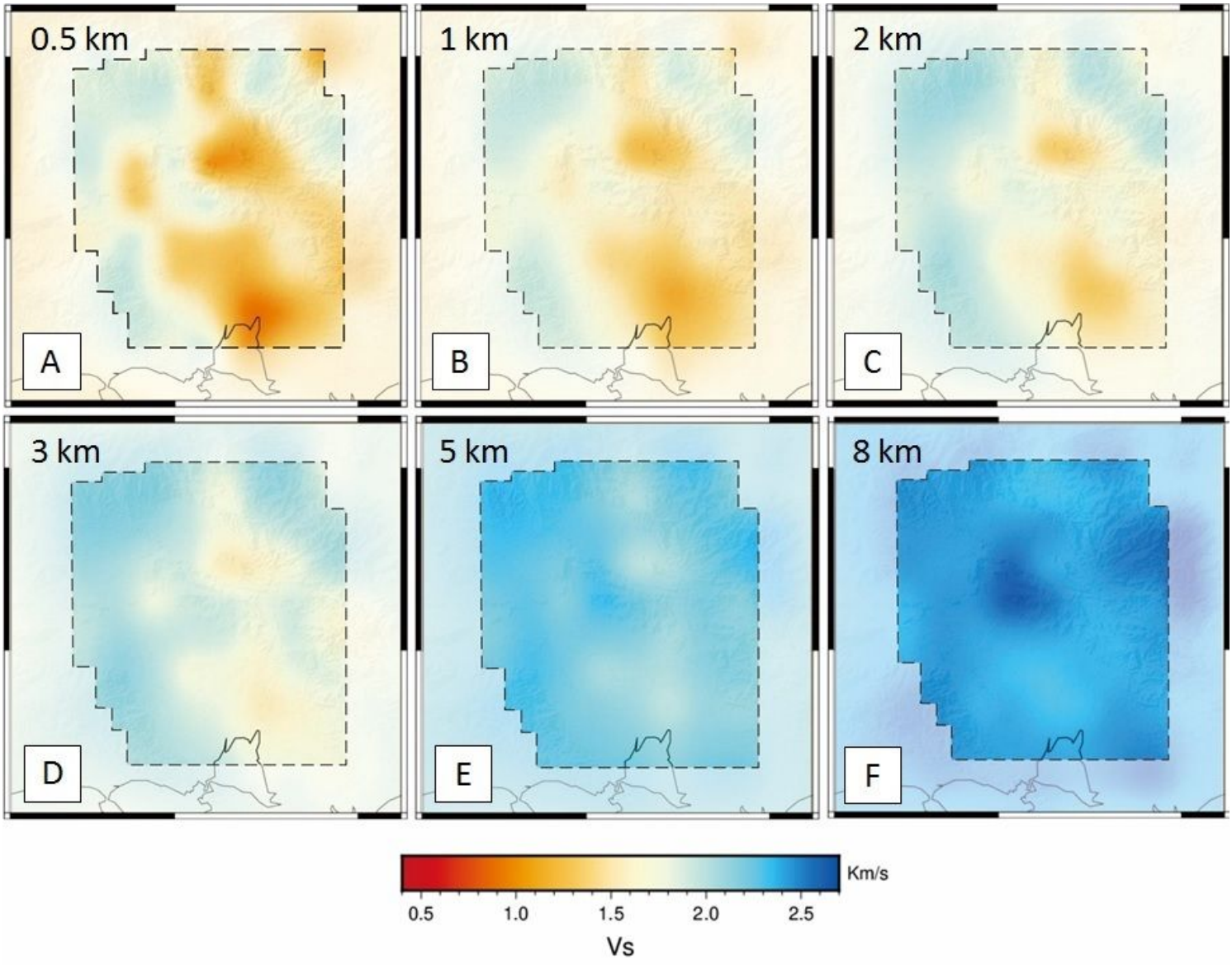

Figure 6

Shear wave velocity (Vs) maps at various depths, (A) 0.5 km, (B) 1 km, (C) 2 km, (D) 3 km, (E) 5 km, and (F) 8 km.

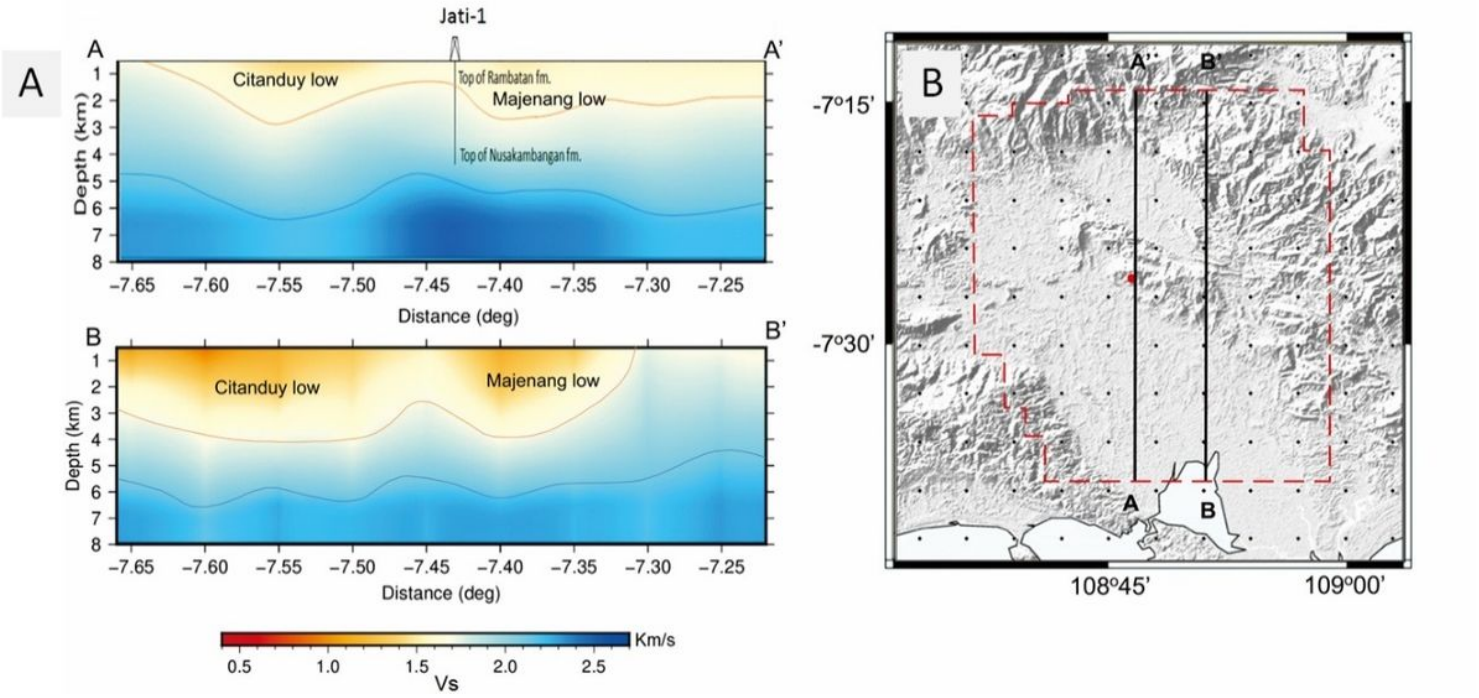

Figure 7

A Vertical cross-section of Vs structure for lines A-A' and B-B' at longitudes 107.776o and 108.85o; B Position of lines A-A' and B-B' on the map is denoted by black lines, the red dashed lines are the limits of the ANT tomographic resolution, and the red dot is the location of the Jati-1 well.

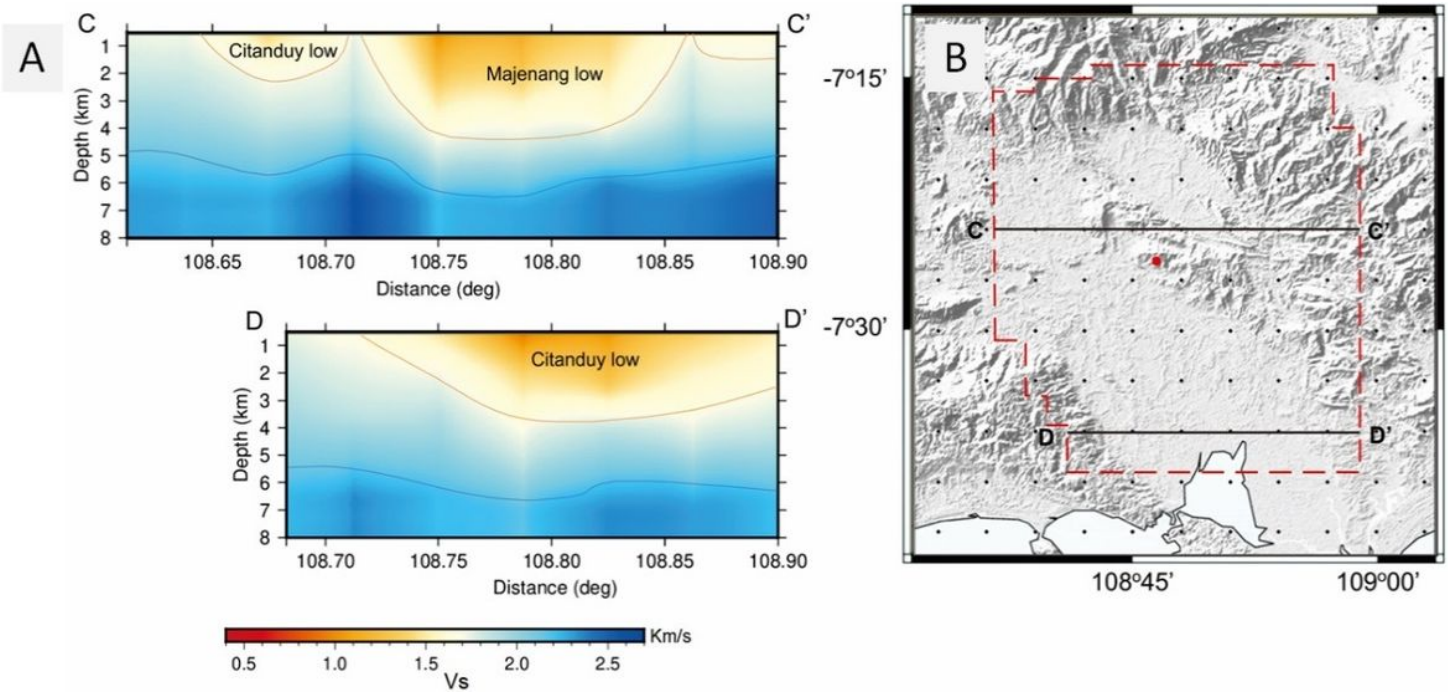

Figure 8

A Vertical cross-section of Vs structure for lines C-C' at latitude -7.4o and lines D-D' at latitude -7.6o; B Position of lines C-C' and D-D' are shown on the map by a black line black; the red dashed line is the

boundary resolution of ANT tomography, and the red dot is the location of the Jati-1 well

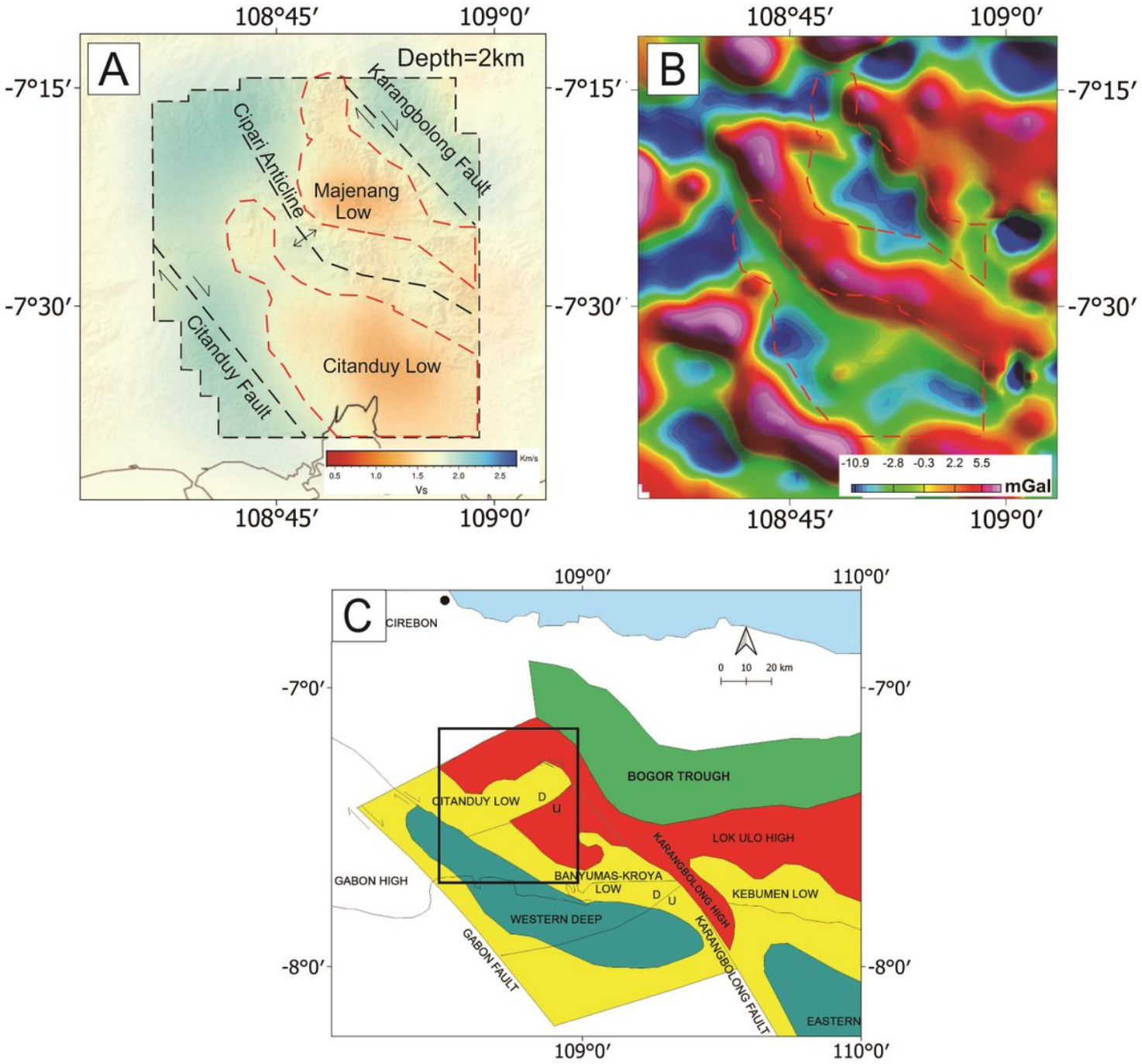

Figure 9

Comparison of results of the ANT in this study with gravity and geological studies. A Tomogram model of Vs at a depth of 2 km and interpretation of the structure and delineation. The area within the dashed black lines represents the resolution limit of the ANT method. The two dashed red lines of low Vs indicate the Majenang Low and the Citanduy Low, separated by the Cipari Anticline. The Citanduy Fault located SW and the Karangbolong Fault located NE, according to Fig. 9C; B The residual bouguer anomaly map (modified from Hidayat et al. 2020); the dashed red line depicted in Fig. 9A shows low Vs delineation; C

Configuration of Miocene structure in the southern Central Java (modified from Muchsin et al. 2002). The black square is the study area, utilizing ANT

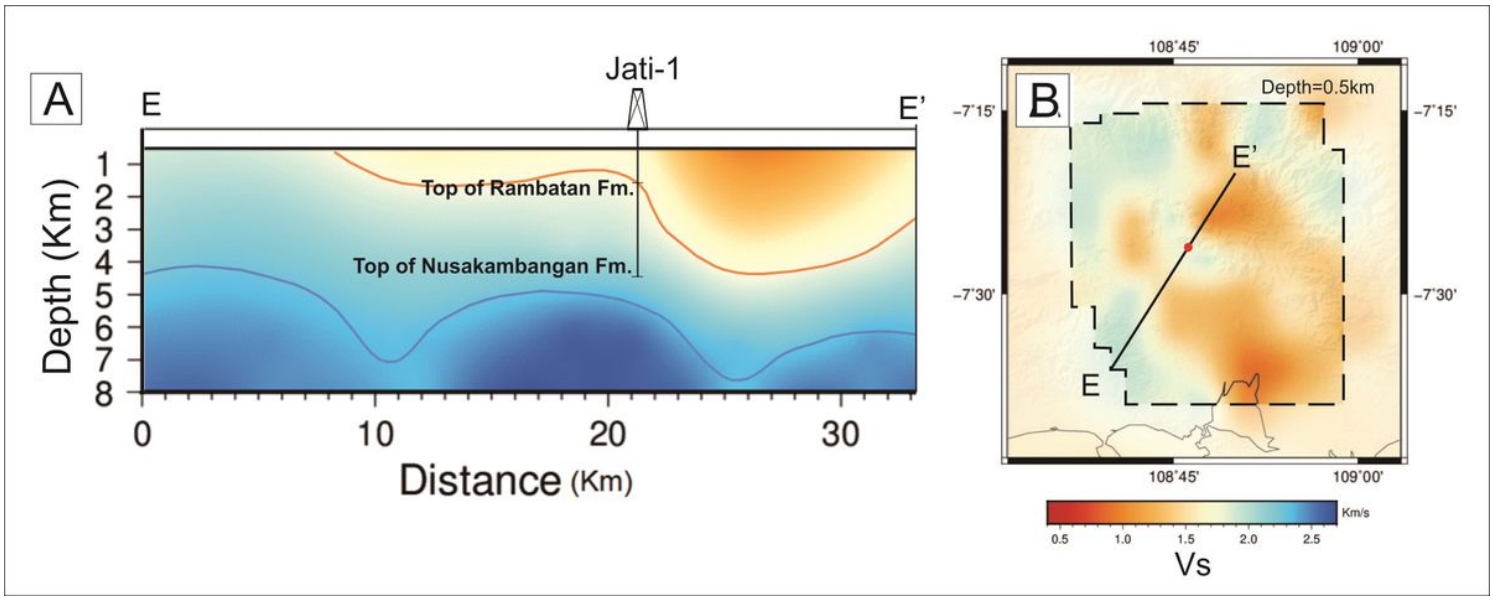

Figure 10

A The vertical section of Vs structure passing through Jati-1 well in the seismic cross-section (E-E'); B Vs structure at a depth of 0.5 km. Blue and red color indictes high and low value of Vs.

Supplementary Files

This is a list of supplementary files associated with this preprint. Click to download.

- supplementarymaterialANTBanyumasIndonesia.docx